

Surface Wind Direction Variability

Author(s): Larry Mahrt

Source: *Journal of Applied Meteorology and Climatology*, Vol. 50, No. 1 (January 2011), pp. 144-152

Published by: American Meteorological Society

Stable URL: <https://www.jstor.org/stable/10.2307/26174010>

REFERENCES

Linked references are available on JSTOR for this article:

[https://www.jstor.org/stable/10.2307/26174010?seq=1&cid=pdf-](https://www.jstor.org/stable/10.2307/26174010?seq=1&cid=pdf-reference#references_tab_contents)
[reference#references_tab_contents](#)

You may need to log in to JSTOR to access the linked references.

JSTOR is a not-for-profit service that helps scholars, researchers, and students discover, use, and build upon a wide range of content in a trusted digital archive. We use information technology and tools to increase productivity and facilitate new forms of scholarship. For more information about JSTOR, please contact support@jstor.org.

Your use of the JSTOR archive indicates your acceptance of the Terms & Conditions of Use, available at <https://about.jstor.org/terms>



American Meteorological Society is collaborating with JSTOR to digitize, preserve and extend access to *Journal of Applied Meteorology and Climatology*

JSTOR

Surface Wind Direction Variability

LARRY MAHRT

Oregon State University, Corvallis, Oregon

(Manuscript received 18 May 2010, in final form 16 August 2010)

ABSTRACT

Common large shifts of wind direction in the weak-wind nocturnal boundary layer are poorly understood and are not adequately captured by numerical models and statistical parameterizations. The current study examines 15 datasets representing a variety of surface conditions to study the behavior of wind direction variability. In contrast to previous studies, the current investigation directly examines wind direction changes with emphasis on weak winds and wind direction changes over smaller time periods of minutes to tens of minutes, including large wind direction shifts. A formulation of the wind direction changes is offered that provides more realistic behavior for very weak winds and for complex terrain.

1. Introduction

Motions on scales just larger than the turbulence are always present (Anfossi et al. 2005) and cause substantial wind direction variation when the large-scale wind is weak. Such unpredictable wind direction changes cause complex transport of contaminants that are not adequately captured in models. Difficulties modeling wind variability is demonstrated in Belušić and Güttsler (2010). Wind direction changes include gradual meandering of the wind direction (Kristensen et al. 1981; Hanna 1983; Etling 1990) or common sudden wind direction shifts (Mahrt 2008). The physics of sudden wind direction changes is poorly understood, but candidate influences are briefly surveyed by Mahrt (2007b). Contributions include steepening gravity waves, density currents, pulses of drainage flow, and numerous other more complex signatures.

The inverse relationship of the wind direction variability to the mean wind speed has been generalized by Joffre and Laurila (1988) and Hanna (1990). Joffre and Laurila (1988) examine the influence of mesoscale motions in terms of an index based on the autocorrelation function for wind speed. Davies and Thomson (1999) provide further generalization by matching weak-wind and strong-wind formulations and considering the dependence on averaging time.

In addition to the usual information on the standard deviation of wind direction, information on sudden wind direction shifts is of considerable interest to a number of practical problems. Unpredicted wind direction shifts lead to poor prediction of transport of contaminants. Sudden wind direction changes reduce the efficiency of wind machines and increase wind-machine fatigue. This study examines the statistics of wind direction changes as a function of wind speed, stability, height above ground, and averaging time for 15 sites ranging from homogeneous to complex topography. One goal of this study is to formulate the distribution of such changes for a variety of surface types, which might be of use in evaluation of numerical models, including dispersion models. In contrast to previous studies of the standard deviation of wind direction, the present study directly examines the statistics of change-of-wind direction and focuses on smaller, nonturbulent time scales in the stable boundary layer, ranging from minutes to tens of minutes. These time scales are sometimes referred to as the submeso range. This investigation emphasizes nocturnal conditions, where wind direction variability tends to be greatest, although daytime conditions are briefly considered.

2. Data

Fifteen datasets will be analyzed (Table 1). The primary dataset for this study was collected from a 34-m tower in Fluxes over Snow Surfaces II (FLOSSII), instrumented from 20 November 2002 to 2 April 2003. The tower site is located over a local flat grass surface within the North

Corresponding author address: Larry Mahrt, COAS, Oregon State University, Corvallis, OR 97330.
E-mail: mahrt@nwra.com

TABLE 1. The location, surface type, number of levels, primary measurement height, and sample size. The reported sample size of the EBEX and Iowa networks is the duration of the field program multiplied by the number of stations. The citations in the last column can be found in the references section; MR refers to the Mary's River site, which includes data in the subcanopy (sc) and at the 28-m level above the canopy. Here, VRBL refers to heavily burned pine and new emerging understory.

Site	Surface	Levels	z	Sample size	References
FLOSSII	Grass	7	2	4 months	Mahrt and Vickers (2006)
CASES-99	Grass	7	5	4 weeks	Poulos et al. (2001)
Iowa	Crops	1	2	8 months	Kustas et al. (2004)
MR sc	20-m fir	1	27	7 months	Thomas et al. (2008)
MR 28	20-m fir	1	5	7 months	Thomas et al. (2008)
Young pine	3-m pine	1	8	1 yr	Schwarz et al. (2004)
Mature pine	15-m pine	1	28	1 yr	Schwarz et al. (2004)
Burn	VRBL	1	5	1 yr	Mahrt (2006)
EBEX	Cotton	1	5	5 months	Oncley et al. (2007)
Juniper	Juniper	1	3	6 months	Mahrt (2006)
PAFEX	Urban	1	9.5	3 weeks	Fernando et al. (2001)
Microfronts	Grass	2	3	3 weeks	Mahrt et al. (1998)
Dutch CASES-99	Grass	2	3	4 weeks	van de Wiel et al. (2003)
ASIT	Sea	2	5	3 months	Edson et al. (2004)
Alaska	Snow	1	2	3 months	Mahrt (2007a)

Park basin of northern Colorado. The grass is often covered by a thin snow layer during the experiment period. This study is based on fast-response data collected at 1, 2, 5, 10, 15, 20, and 30 m with Campbell Scientific Instruments, Inc., 3D sonic anemometers (CSAT3). We will emphasize the FLOSSII data because they include vertical structure for a multimonth period and are intermediate between sites that are relatively homogenous over large areas and sites in complex terrain. We will primarily analyze 1-min-averaged data, which filters out the turbulence for almost all of the nocturnal records. Larger averaging times up to 16 min will also be used.

Details for the 14 other sites can be found in the citations listed in the last column of Table 1. The vegetation for the burn site consists of scattered burned ponderosa pine trunks and emerging vegetation less than 1 m high. The Phoenix Air Flow Experiment II (PAFEXII) was conducted at the Falcon Regional Airport, Phoenix, Arizona, in the summer of 1998. The surface consists of very sparse matted dead grass with an effective height of less than 5 cm. Much of the surface area is sand.

3. Wind-direction change

The usual computation of the standard deviation of the wind direction must contend with discontinuities in the time series at 0° – 360° . That is, with northerly flow, small changes of wind direction can lead to nearly 360° changes of wind direction. These discontinuity crossings in the time series of wind direction become common with weak winds. Such problems are extensively discussed in Farrugia et al. (2009) along with approximate solutions. The current study focuses on wind direction changes

between subsequent time intervals, which do not encounter such difficulties. Computed wind direction changes are reduced by 360° if they exceed 180° , or are increased by 360° if they are more negative than -180° , such that they lie within the range of -180° – $+180^\circ$. Approximate reversals of wind direction would correspond to changes close to -180° or close to $+180^\circ$. In such cases, the magnitude of the wind direction change is more significant than the sign of the wind direction change.

The following procedure is used for estimation of wind direction changes in this study. Wind direction (Wdir) is computed from wind components averaged over periods of $\tau_F = 1$ -, 2-, 4-, 8-, or 16-min periods. The wind direction change, $\delta_t(\text{Wdir})$, is computed as the difference of wind direction between adjacent averaging periods, that is, the difference over a window of width $2\tau_F$. This window is sequentially advanced by 1 min between evaluations. The window overlap increases with increasing τ_F , but provides the same number of samples for each window width and reduces significant sampling problems at large window widths. Although greater overlapping better captures the maximum wind direction shift, this dependence of overlap on τ_F does not affect the conclusions of this study. For example, implementing nonoverlapping windows for all values of τ_F led to significantly larger scatter in the wind direction statistics, but did not reveal any systematic differences from the current approach of sequentially advancing the window by 1 min for all values of τ_F .

We will relate the wind direction changes to the speed of the window-averaged wind vector. As a result, the relationship between direction variability and the wind speed is more localized than the usual calculation of the standard deviation of wind direction over the entire

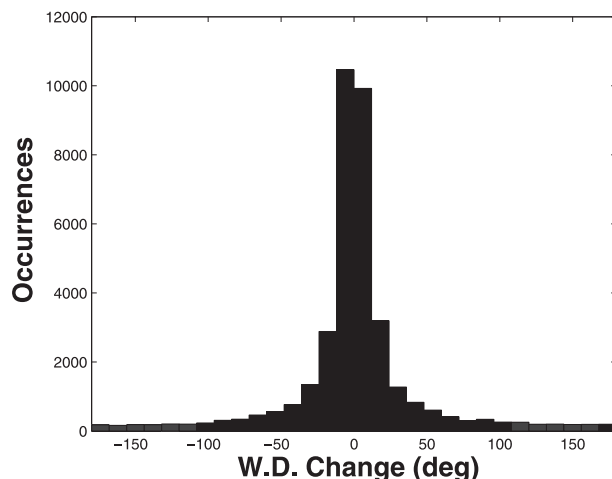


FIG. 1. Frequency distribution of changes of the 1-min wind direction at 2 m for nocturnal FLOSSII (38 920 values).

record. Despite the fundamental differences between previous calculations and the present calculation of wind direction variability, both approaches yield an approximate inverse-linear relationship to mean wind speed, subject to some important exceptions.

4. Wind-direction variability

Results in this section refer to nocturnal conditions and 1-min differences over a 2-min window unless otherwise noted. We initially concentrate on the FLOSSII data with the recognition that the wind direction characteristics vary between sites. Two choices of metrics for wind direction change are the average absolute value and the standard deviation of the wind direction change, $\sigma_{\delta\text{wd}}$. The wind direction change, $\delta_t(\text{Wdir})$, averages less than 1° for FLOSSII as well as for most of the other datasets, since the wind direction change shows little preference for clockwise or counterclockwise rotation with time, as is evident in the distributions in Figs. 1 and 2. Since the mean wind direction change is near zero, the average magnitude of the wind direction change is proportional to the standard deviation of $\delta_t(\text{Wdir})$, symbolized as $\sigma_{\delta\text{wd}}$. For example, for a Gaussian distribution with zero mean, the average absolute value of the wind direction change would be $\sigma_{\delta\text{wd}}\sqrt{2/\pi}$. Here, we choose $\sigma_{\delta\text{wd}}$ as the metric and include examination of the skewness and kurtosis of the wind direction change in later sections.

The wind direction variability, $\sigma_{\delta\text{wd}}$, increases rapidly with decreasing wind speed for wind speeds less than about 2 m s^{-1} (Fig. 2). With decreasing wind speed, always-present submeso motions (on scales of minutes or tens of minutes) significantly enhance the wind direction variability. For wind speeds substantially stronger than the

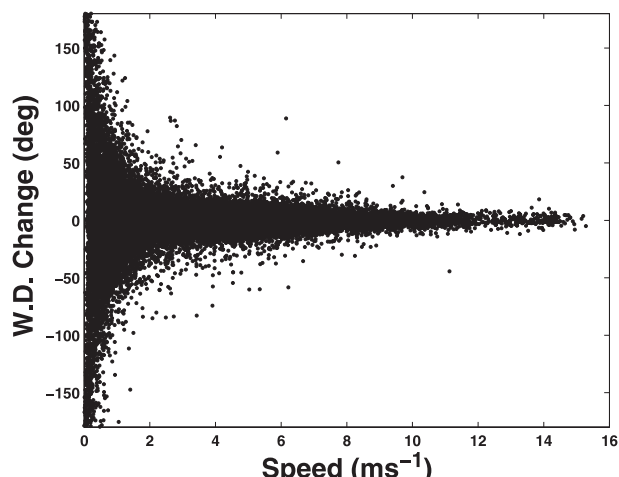


FIG. 2. The change of the 1-min wind direction at 2 m as a function of wind speed for nocturnal FLOSSII.

amplitude of submeso motions, the submeso flow causes only small changes of the wind direction.

a. Dependence on wind speed for different averaging times

Since the wind direction variability is strongly inverse related to the mean wind speed, we partition the data into different wind speed intervals, δV . In this analysis, the wind speed intervals are chosen to be 0.25 m s^{-1} between 0 and 2 m s^{-1} , and 1 m s^{-1} for speeds greater than 2 m s^{-1} . The greater wind speed resolution is needed for very weak winds where the wind direction variability changes rapidly with changing speed. Averages will be computed for all intervals that have at least 20 samples.

Figure 3 shows the dependence of $\sigma_{\delta\text{wd}}$ on wind speed for different averaging times for the nocturnal FLOSSII data. The wind direction variability does not depend significantly on averaging time for very weak ($<1 \text{ m s}^{-1}$) or stronger ($>3 \text{ m s}^{-1}$) wind speeds. However, for intermediate speeds between 1 and 3 m s^{-1} , the wind direction variability doubles as the averaging time is increased from 1 to 16 min (Fig. 3). Similar increases also occur for those datasets over flatter terrain, but generally not over complex terrain (Table 2). The physics of this scale dependence is not understood.

For some of the complex-terrain sites, the wind direction variability ($\sigma_{\delta\text{wd}}$) increases with increasing averaging time for weaker wind speeds, but decreases with increasing averaging time for stronger wind speeds (not shown). The transition wind speed for this reversal of scale dependence is given in the fourth column of Table 2. Relative to flatter terrain, this reversal implies a shift to smaller time scales for stronger wind speeds in complex terrain, perhaps because of terrain-induced eddies. As an aside, the

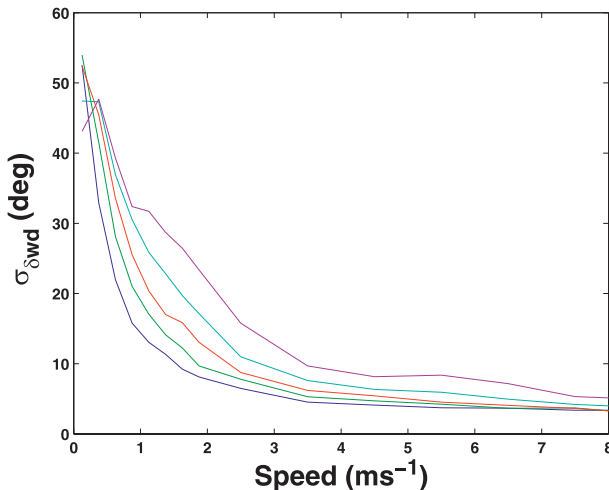


FIG. 3. The dependence of the bin-averaged $\sigma_{\delta\text{wd}}$ on averaging time as a function of wind speed for different averaging widths for the FLOSSII 2-m nocturnal winds for 1- (blue), 2- (green), 4- (red), 8- (cyan), and 16-min (magenta) averaging widths. The wind-direction variability increases monotonically with averaging width.

rate of wind direction change (e.g., degrees per min), computed by dividing the wind direction change by τ_F , does not increase with increasing wind direction change.

b. Dependence on height and stability

The dependence of the wind direction variability on wind speed shows little dependence on height (Fig. 4). That is, the decrease of wind direction variability with height is mainly due to increasing wind speed with height and, therefore, reasonably well predicted by wind speed alone, without information on height. This simplicity is partly due to the near independence of the strength of the submeso motions with height. Similar height dependence is found for the Cooperative Atmosphere-Surface Exchange Study-1999 (CASES-99) data. The dependence of the nocturnal wind direction variability on stability is also largely included through the dependence on wind speed; that is, for the current primarily fair-weather datasets, the stability and wind speed are strongly inversely correlated.

The magnitude of the wind direction variability, for a given wind speed interval, is significantly larger in the daytime for the CASES-99 data (Fig. 5), partly because of wind direction changes associated with large boundary layer convective eddies. In spite of increased wind direction variability in the daytime, compared to nocturnal conditions for the same wind speed, the wind direction variability is greater at night because of weaker nocturnal winds and the general increase of wind direction variability with decreasing wind speed. The differences between day and night are much smaller for FLOSSII than CASES-99 because of the small surface heat flux in

TABLE 2. Between-site differences of the wind-direction variability. Nocturnal values of $\sigma_{\delta\text{wd}}$ ($^{\circ}$) for 1-min (first column) and 16-min (second column) averages for the wind speed interval $1.75\text{--}2.00 \text{ m s}^{-1}$; typically the wind speed interval of near-maximum dependence on averaging time. Daytime values are reported in the parentheses. Also shown are the transition wind speed (ws rev; m s^{-1}) for reversal of the dependence of $\sigma_{\delta\text{wd}}$ on averaging time (see text), and the skewness and kurtosis for 1-min averaging for the $3\text{--}4 \text{ m s}^{-1}$ wind speed interval; generally the wind speed interval of near-maximum values. Since wind speeds rarely exceed a few meters per second in the MR sc, one set of values is reported for the entire wind speed range. The first seven sites are over relatively flat terrain, FLOSSII and EBEX are locally simple terrain in broad valleys bordered by large mountain ranges, and the last six stations are within complex terrain.

Site	σ (1 min)	σ (16 min)	Ws rev	Skewness	Kurtosis
ASIT	4 (5)	12 (10)		7 (4)	50 (21)
Alaska	3 (4)	8 (8)		3 (2)	17 (8)
Iowa	3 (13)	6 (13)		1.5 (1.5)	5 (6)
Microfronts	3 (13)	8 (13)		6 (2)	27 (5)
CASES-99	3 (15)	9 (13)		3 (1)	10 (4)
Dutch	3 (14)	16 (14)		5 (2)	23 (5)
PAFEX	6 (14)	14 (17)		5 (2)	22 (8)
FLOSSII	9 (10)	23 (21)		4 (2)	30 (12)
EBEX	5 (10)	13 (12)	4	3 (2)	10 (7)
MR sc	12 (10)	6 (13)		2 (2)	10 (8)
MR 38 m	8 (14)	5 (10)	1 (0)	4 (1.3)	20 (4.5)
Juniper	8 (15)	9 (16)	2 (4)	3.5 (1.5)	25 (5)
Mature pine	13 (15)	18 (17)	4 (3)	9 (3.5)	125 (45)
Burn	9 (14)	10 (15)	2 (3.5)	2.5 (1.5)	20 (4)
Young pine	17 (19)	15 (18)	(1.5)	5 (3)	56 (24)

FLOSSII as a result of low winter sun angles and frequent snow cover. For the other sites for a given wind speed, the wind direction variability is generally augmented significantly in the daytime with significant surface heating.

5. Between-site comparisons

Since the dependence of wind direction variability on the wind speed is not sensitive to height above ground, the variation between sites can be examined without major concern for the exact height of the measurements. However, submeso motions and associated wind direction variability are significantly site dependent, partly because of greater submeso activity in complex terrain. This expectation is consistent with greater crosswind fluctuations over complex terrain found by Hanna (1983), Vickers and Mahrt (2007), and others. Table 2 and Fig. 6 show enhanced wind direction variability over complex terrain for the nocturnal 1-min-averaged flow. Among the complex-terrain sites, the burned site is characterized by the smallest wind direction variability, apparently because of some channeling by the narrow valley. The wind speed interval $1.75\text{--}2 \text{ m s}^{-1}$ was chosen as a reference interval

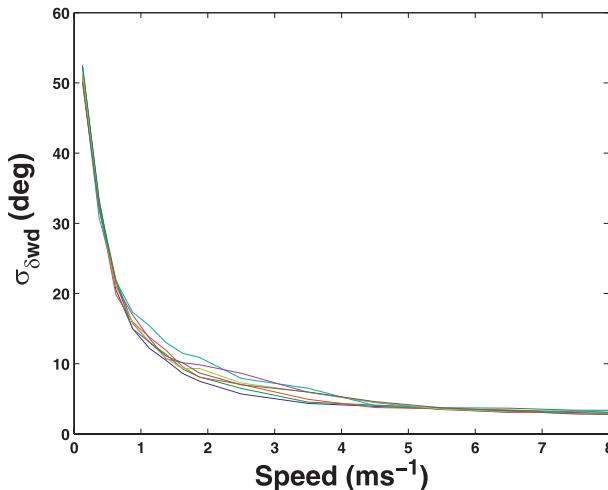


FIG. 4. The dependence of the bin-averaged $\sigma_{\delta\text{wd}}$ for 1-min averaging as a function of wind speed for different measurement levels corresponding to 1 (blue), 2 (green), 5 (red), 10 (cyan), 15 (magenta), 20 (yellow), and 30 m (black).

in Table 2, since this interval is often close to the wind speed of strongest dependence on averaging time. This choice best reveals the between-site dependence of the wind direction variability on averaging time.

The 1-min wind direction variability for sites in complex terrain (Fig. 6, dashed lines) is substantially greater than the direction variability at the flatter sites (Fig. 6, solid lines) for all of the wind speed intervals. The two flattest sites, one over snow (red pluses) and one over the sea in the coastal zone (black pluses), have the smallest wind direction variability along with three grassland sites. The topographical characteristics of the FLOSSII (red circles) and Energy Balance Experiment (EBEX; green dashed) sites are between those of the flatter and complex-terrain sites in that the FLOSSII and EBEX sites are located in relatively flat broad valleys bounded by mountain ranges. These sites exhibit intermediate values of $\sigma_{\delta\text{wd}}$.

The two sites located immediately downwind from the Cascade Mountains (red and cyan dashed lines) show increasing wind direction variability with stronger winds, presumably because of inducement of instabilities by the mountains with stronger winds. The events responsible for such large wind direction variability at the young pine site (cyan dashed) were often associated with sequential wind shifts in the same direction (rotation) as opposed to isolated shifts or reversals back and forth between two wind regimes. For example, one event consisted of counter-clockwise rotation of about $130^\circ \text{ min}^{-1}$ for three cycles of rotation, corresponding to a period of about 3 min, with an almost-steady wind speed of 6 m s^{-1} . For the entire year, there was no obvious preference between clockwise and counterclockwise rotation of the wind direction. For

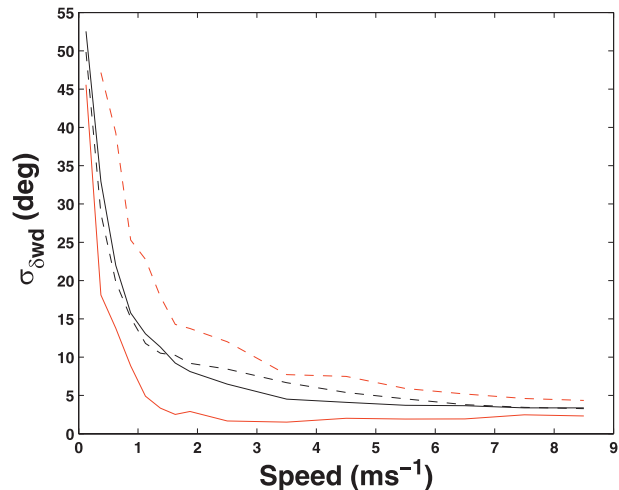


FIG. 5. Dependence of the near-surface 1-min wind-direction variability on wind speed for FLOSSII nocturnal (black), FLOSSII daytime (black dashed), CASES-99 nocturnal (red), and CASES-99 daytime (red dashed).

nocturnal conditions, about 2% of all 1-min wind direction changes at the young pine site for wind speed greater than 5 m s^{-1} are greater than 90° . The frequency of such large wind direction changes decreases with increasing τ_F , indicating the small-scale characteristics of these changes at this site downwind from the Cascade Mountains.

Skewness and kurtosis; event nature

The skewness and kurtosis of the wind direction change can be strongly influenced by events. The values of skewness and kurtosis are shown in Table 2 for the wind speed interval $3\text{--}4 \text{ m s}^{-1}$, where the skewness and kurtosis generally reach near-maximum values with respect to variation with wind speed. The skewness does not vary systematically between flat- and complex-terrain sites. However, the kurtosis is generally larger for complex-terrain sites, reflecting the more event behavior of wind direction changes. For very large values of the kurtosis, the exact values may not be significant beyond the fact that the values of the kurtosis are large. Both the skewness and kurtosis are generally smaller for daytime conditions compared to nocturnal conditions. At most sites, the skewness does not vary systematically with averaging time. There are exceptions to all of the above tendencies.

The nocturnal dependence of the skewness and kurtosis on wind speed for FLOSSII (Fig. 7) is typical of the various sites (Table 2), except that the kurtosis for FLOSSII is more erratic than for the larger one-year datasets and for the datasets from flatter sites. The skewness of the wind direction change is near 0 or slightly negative for very weak winds ($<0.5 \text{ m s}^{-1}$) for all the sites, both day

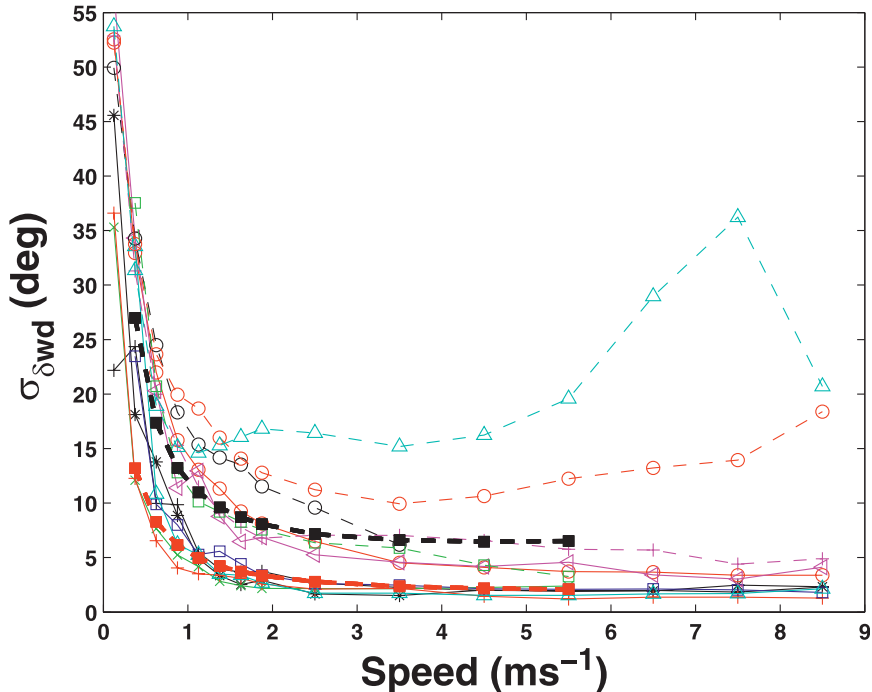


FIG. 6. Dependence of the near-surface nocturnal 1-min wind-direction variability on wind speed for FLOSSII (red, circles), CASES-99 (black, asterisks), ASIT (black, +), Alaska (red, +), Iowa (green, asterisk), Dutch CASES-99 (blue, squares), microfronts (cyan, triangles), PAFEX (magenta, triangles), Mary's River (black dashed, circles), mature pine (red dashed, circles), juniper (magenta dashed, +), EBEX (green dashed, squares), and young pine (cyan dashed, triangles). The thick dashed lines with markers are model values [Eq. (4)] for flatter terrain (thick red dashed) and complex terrain (thick black dashed). Although individual lines are sometimes difficult to discern, the grouping of lines is discussed in the text.

and night. The skewness increases with wind speed for all of the sites, generally reaching a maximum of 3 or more at wind speeds between 1 and 5 m s^{-1} . The general positive skewness of the wind direction change for significant wind for all of the sites indicates that the strongest wind direction changes tend to be clockwise. Such wind direction changes would be consistent with mixing events and downward momentum transport in the presence of Ekman turning with height. Evidently, recovering from these events associated with counterclockwise rotation of the wind direction occurs more slowly without large direction shifts. Nonetheless, the average value of the wind direction change over all of the data is near zero. There is not a preference for clockwise rotation compared to counterclockwise, only that the clockwise rotation is, on average, more eventlike (smaller duration, but faster turning rate).

For all of the sites, the kurtosis is generally near the Gaussian value of 3 for very weak winds and usually increases significantly with wind speed, often to values greater than 20. The wind speed corresponding to the maximum kurtosis varies between sites, but is usually

close to the wind speed of maximum skewness for that site. The small kurtosis for weak winds reflects common random-like variation of wind direction, while more significant wind speeds include occasional large wind direction changes. Wind direction changes greater than 90° , where the component of the wind in the original wind direction reverses sign, is a noteworthy event for dispersion transport. For all of the sites, the probability of wind direction changes greater than 90° increases rapidly when the wind speed decreases to values less than about 1 m s^{-1} , as is shown for FLOSSII in Fig. 7.

6. Formulation

There is no history for parameterization of $\sigma_{\delta\text{wd}}$. We first briefly consult previous formulations of σ_θ . The wind direction variability is often modeled as an inverse dependence on the mean wind speed (introduction), sometimes motivated by the approximation (Davies and Thomson 1999)

$$\sigma_\theta \approx \sigma_v/V, \quad (1)$$

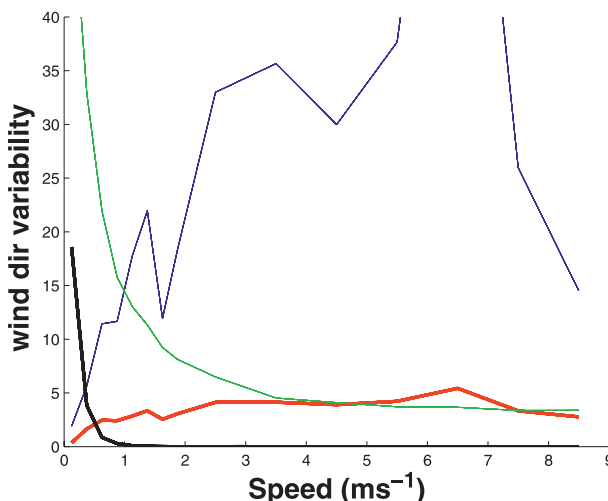


FIG. 7. Kurtosis (blue) and skewness (red) of the 1-min wind-direction change for nocturnal FLOSSII 2 m as a function of wind speed. Also shown are $\sigma_{\delta\text{wd}}$ (green) and the probability of wind shifts greater than 90° between subsequent 1-min windows (black). One of the kurtosis values is offscale. The numerical values on the y axis apply to all four variables, which are nondimensional, except that $\sigma_{\delta\text{wd}}$ is expressed in degrees.

where σ_θ is the standard deviation of the wind direction, V is the speed of the vector-averaged wind, and v is the wind component perpendicular to the direction of the mean wind. This relationship is a useful approximation if the magnitude of v remains small in comparison with V , that is, if the wind direction variability is small. The quantity σ_v is often replaced by a constant, which is found to fit the data well for many situations. If turbulence was excluded from σ_v , this behavior would be consistent with submeso–mesoscale kinetic energy that is independent of wind speed, as implied by the observations of Anfossi et al. (2005) and others. Davies and Thomson (1999) included a turbulent contribution to σ_θ . This contribution is independent of wind speed based on the approximation that the turbulent part of σ_v is proportional to wind speed for near-neutral conditions, such that

$$\sigma_\theta = \beta/V + C, \quad (2)$$

where C is estimated from turbulence similarity theory for neutral conditions and is inversely related to surface roughness.

Our study includes extremely weak winds such that relating σ_θ or $\sigma_{\delta\text{wd}}$ to the inverse of wind speed would lead to large unrealistic values of wind direction change, approaching infinity as V vanishes. The actual upper bound of $\sigma_{\delta\text{wd}}$ is 180° , corresponding to 180° reversals of the wind direction between all sequential averages. Replacing the speed of the vector-averaged wind with averaged wind

speed reduces the prediction of unrealistically large wind direction variability at very weak winds; however, numerical models of the atmosphere provide only the speed of the grid-averaged wind vector.

The unrealistic behavior with vanishing mean flow is ameliorated by defining a modified velocity scale

$$V_{\text{mod}} = \sqrt{V^2 + V_{\text{sg}}^2}, \quad (3)$$

where V_{sg} provides empirical limitation to the wind direction variability with vanishing V , and in models is presumably related to the strength of the unresolved submeso motions. For applications in models, V_{sg} must be parameterized.

A generalized prediction of wind direction variability can be written as

$$\sigma_{\delta\text{wd}} = \frac{A}{V_{\text{mod}}} + BV^n, \quad (4)$$

where the first term is a generalized inverse dependence on wind speed and the second term is generalization needed for stronger winds in complex terrain. The quantity V is the numerical value of the speed corresponding to meters per second such that V^n is nondimensional and B is expressed in degrees. Based on subjective fitting of the 1-min averages for the different sites, A is chosen to be $10^\circ \text{ m s}^{-1}$ in Fig. 6 for the theoretical curve representing complex terrain (thick black dashed line) and 5° m s^{-1} for flatter terrain (thick red dashed line). The V_{sg} is chosen to be 0.1 m s^{-1} for both simple and complex terrain. Future improvement could include larger V_{sg} for complex terrain. With vanishing wind speed, Eq. (4) predicts a limiting maximum value of $\sigma_{\delta\text{wd}} = A/V_{\text{sg}}$, which is 100° with current parameter values for complex terrain.

The second term on the right side of Eq. (4) represents the contributions to wind direction variability that do not decrease with increasing wind speed. This might include turbulence wind direction variations that can extend to scales greater than 1 min for strong winds. In addition, the wind direction variability for moderate and stronger winds seems to be significantly enhanced by complex terrain. In fact, topographical generation of wind direction variability may increase with increasing speed of the vector-averaged wind (section 5). In Fig. 6, this term is formulated with $n = 0.5$ and $B = 2^\circ$ for the complex-terrain model and 0.5° for the simple-terrain model.

Equation (4) reduces to the usual inverse dependence on wind speed if $V_{\text{sg}} = 0$, A is constant, and $B = 0$. Despite the generalization represented by Eq. (4), important omissions remain. The model does not include the factor-of-2 increase of wind direction variability for daytime

convective conditions that occurs for short averaging times over relatively flat terrain. This simple model also does not capture the increase of wind direction variability with increasing averaging time for the intermediate wind speeds for the relatively flat-terrain sites. Attempts to generalize the model by specification of parameter values in terms of the averaging time are not practical because this enhancement depends on both wind speed and site topography.

Distributions

A Gaussian distribution of wind direction change can be constructed in terms of the standard deviation predicted by Eq. (4). Such a model will underestimate the frequency of large wind direction changes—crucial information for some practical applications. Unfortunately, the skewness and the kurtosis of the wind direction change vary between sites as well as depend on time of day and wind speed. Collectively considering all of the sites, a conservative nocturnal value of skewness for wind speeds greater than 2 m s^{-1} is 3 with a corresponding kurtosis of 20 for flatter sites and 30 for complex-terrain sites. Smaller values of skewness and kurtosis are needed for very weak winds. For example, the skewness might be chosen to decrease linearly to 0 with vanishing wind speed while the kurtosis decreases to about 3 with vanishing wind speed. That is, the very large wind direction variability for very weak winds can be approximated with a Gaussian distribution, while less common events like wind direction changes for more significant winds require nonzero skewness and large kurtosis, even as a first approximation. The above values of skewness and kurtosis, and the standard deviation based on Eq. (4), provide for construction of a probability distribution, which is left for a future study.

7. Conclusions

The increased variability of the surface wind direction with decreasing mean wind speed is examined here in terms of wind direction change across a differencing window (section 3) in contrast to the usual standard deviation of the wind direction. This study constructed statistics for wind direction change based on 15 sites of varying surface type and terrain configuration. These statistics were used to formulate the wind direction change (section 6) that includes the probability of large wind direction shifts for a given mean wind speed and surface setting. This formulation includes the strong influence of submeso motions on wind direction variability for weak large-scale flow. The large wind direction variability for weak winds implies that emitted particles travel slowly for short distances before changing direction and thus can retain high concentrations in the vicinity of the source.

The decrease of the wind direction variability with height near the surface is well predicted by the dependence of wind direction variability on wind speed, without specific information on height. The wind direction variability is greater over complex terrain for small averaging times of minutes; however, this difference becomes undetectable for averaging times greater than 10 min, implying that the complex terrain induces greater wind direction variability, mainly on smaller time scales. Although the wind direction variability for a given wind speed is, on average, greater for unstable conditions, the probability of very weak winds are much greater for stable stratification. As a result, the wind direction variability is generally much larger for the nocturnal boundary layer. The kurtosis of wind direction change for significant wind is generally greater for nocturnal conditions compared to daytime conditions and greater for complex terrain compared to flat terrain, reflecting the eventlike nature for such conditions.

The present analysis and the formulations in section 6 still include significant deficiencies. Improved understanding of the physics underlying the wind direction shifts is required.

Acknowledgments. The important comments of Danijel Belušić, Branko Grisogono, and the reviewers are gratefully acknowledged. This material is based upon work supported by NSF Grant ATM-0607842 and ARO Contract W911FN05C0067.

REFERENCES

- Anfossi, D., D. Oetti, G. Degrazia, and A. Goulart, 2005: An analysis of sonic anemometer observations in low wind speed conditions. *Bound.-Layer Meteor.*, **114**, 179–203.
- Belušić, D., and I. Güttler, 2010: Can mesoscale models reproduce meandering motions? *Quart. J. Roy. Meteor. Soc.*, **136**, 553–565.
- Davies, B. M., and D. J. Thomson, 1999: Comparisons of some parameterizations of wind direction variability with observations. *Atmos. Environ.*, **33**, 4909–4917.
- Edson, J. B., R. Crofoot, W. R. McGillis, and C. J. Zappa, 2004: Investigations of flux-profile relationships in the marine atmospheric boundary layer during CBLAST. *Extended Abstracts, 16th Symp. on Boundary Layers and Turbulence*, Portland, ME, Amer. Meteor. Soc., 8.2. [Available online at <http://ams.confex.com/ams/pdfpapers/78615.pdf>.]
- Etling, D., 1990: On plume meandering under stable stratification. *Atmos. Environ.*, **24A**, 1979–1985.
- Farrugia, P., J. Borg, and A. Micallef, 2009: On the algorithms used to compute the standard deviation of wind direction. *J. Appl. Meteor. Climatol.*, **48**, 2144–2151.
- Fernando, H. J. S., S. M. Lee, J. Anderson, M. Princevac, E. Pardyjak, and S. Grossman-Clarke, 2001: Urban fluid mechanics, air circulation and contaminant dispersion in cities. *Environ. Fluid Mech.*, **1**, 107–164.

- Hanna, S. R., 1983: Lateral turbulence intensity and plume meandering during stable conditions. *J. Climate Appl. Meteor.*, **22**, 1424–1430.
- , 1990: Lateral dispersion in light wind stable conditions. *Nuovo Cimento*, **13C**, 889–894.
- Joffre, S. M., and T. Laurila, 1988: Standard deviations of wind speed and direction from observations over a smooth surface. *J. Appl. Meteor.*, **27**, 550–561.
- Kristensen, L., N. Jensen, and E. L. Peterson, 1981: Lateral dispersion of pollutants in a very stable atmosphere: The effect of the meandering. *Atmos. Environ.*, **15**, 837–844.
- Kustas, W., F. Li, J. Jackson, J. Prenger, J. MacPherson, and M. Wolde, 2004: Effects of remote sensing pixel resolution on modeled energy flux variability of croplands in Iowa. *Remote Sens. Environ.*, **92**, 535–547.
- Mahrt, L., 2006: Variation of surface air temperature in complex terrain. *J. Appl. Meteor. Climatol.*, **45**, 1481–1493.
- , 2007a: The influence of nonstationarity on the turbulent flux-gradient relationship for stable stratification. *Bound.-Layer Meteor.*, **125**, 245–264.
- , 2007b: Weak-wind mesoscale meandering in the nocturnal boundary layer. *Environ. Fluid Mech.*, **7**, 331–347.
- , 2008: Mesoscale wind direction shifts in the stable boundary layer. *Tellus*, **60A**, 700–705.
- , and D. Vickers, 2006: Extremely weak mixing in stable conditions. *Bound.-Layer Meteor.*, **119**, 19–39.
- , J. Sun, W. Blumen, A. Delany, G. McClean, and S. Oncley, 1998: Nocturnal boundary-layer regimes. *Bound.-Layer Meteor.*, **88**, 255–278.
- Oncley, S. P., and Coauthors, 2007: The Energy Balance Experiment EBEX-2000. Part 1: Overview and energy balance. *Bound.-Layer Meteor.*, **123**, 1–28.
- Poulos, G. S., and Coauthors, 2001: CASES-99: A comprehensive investigation of the stable nocturnal boundary layer. *Bull. Amer. Meteor. Soc.*, **83**, 555–581.
- Schwarz, P., B. Law, M. Williams, J. Irvine, M. Kurpius, and D. Moore, 2004: Climatic versus biotic constraints on carbon and water fluxes in seasonally drought-affected ponderosa pine ecosystems. *Global Biogeochem. Cycles*, **18**, 1029–1037.
- Thomas, C., J. G. Martin, M. Goeckede, M. B. Siqueira, T. Foken, B. E. Law, H. W. Loescher, and G. Katul, 2008: Estimating daytime subcanopy respiration from conditional sampling methods applied to multi-scalar high frequency turbulence time series. *Agric. For. Meteor.*, **148**, 1210–1229.
- Van de Wiel, B. J. H., A. F. Moene, O. K. Hartogensis, H. A. R. De Bruin, and A. A. M. Holtslag, 2003: Intermittent turbulence in the stable boundary layer over land. Part III: A classification for observations during CASES-99. *J. Atmos. Sci.*, **60**, 2509–2522.
- Vickers, D., and L. Mahrt, 2007: Observations of the cross-wind velocity variance in the stable boundary layer. *Environ. Fluid Mech.*, **7**, 55–71.